Enhanced productivity on the Iberian margin during glacial/interglacial transitions revealed by barium and diatoms

J. THOMSON[1], S. NIXON[1], C. P. SUMMERHAYES[1], E. J. ROHLING[1], J. SCHÖNFELD[2], R. ZAHN[2], P. GROOTES[3], F. ABRANTES[4], L. GASPAR[4] & S. VAQUEIRO[4]

[1]*Southampton Oceanography Centre, Empress Dock, Southampton SO14 3EZ, UK*
[2]*GEOMAR Research Center for Marine Geosciences, Wischhofstr. 1–3, D-24148 Kiel, Germany*
[3]*Leibniz-Labor für Altersbestimmung und Isotopenforschung, Christian-Albrechts Universität, Kiel, Germany*
[4]*Instituto Geologico e Mineiro, Departamento de Geologia Marinha, Estrada da Portela, Zambujal—Alfragide, Portugal*

Abstract: The Portuguese margin is at a critical location for studies of the ocean's behaviour during glacial/interglacial climatic changes, and the rapid accumulation rates of the sediments enable high-resolution palaeoclimatic investigation. The sedimentary record of the past 350 ka has been investigated in a 35 m long core from 3.5 km water depth on the slope at 40°N by geochemical, isotopic and micropalaeontological techniques. The $CaCO_3$ content of this core as a function of time contains significant Milankovitch orbital frequencies of 18.8, 23.7, 38.0 and 100.6 ka, but these are driven primarily by dilution by clay-flux variations rather than by $CaCO_3$ productivity variations. The largest signals in the productivity indicators C_{org}, Ba/Al and diatom abundance are all observed as simultaneous peaks at the oxygen isotope stage boundaries 10/9 and 6/5, with the signal magnitude in the order 10/9>6/5 for all three indicators. Smaller coincident signals in C_{org}, Ba/Al but not diatoms are also observed at the oxygen isotope stage 2/1 boundary. Other less prominent peaks in the C_{org} and Ba/Al profiles occur elsewhere, including Heinrich Event horizons, but these are not always simultaneous and none contain evidence of the dissolution-prone diatom microfossils. The 10/9, 6/5 and 2/1 oxygen isotope stage transitions represent the three most extreme glacial/interglacial sea level rises in the past 350 ky, possibly in the same sequence of magnitude, when sea level rose rapidly by 120+m from glacial low stands to interglacial high stands. The productivity signals at these transitions are contained within <5 ka (including bioturbation).

Keywords: Pleistocene, Iberian margin, sedimentation, oxygen isotopes, barium.

The International Marine Global Change Studies (IMAGES) and the UK NE Atlantic Palaeoceanography and Climate Change (NEAPACC) projects are both concerned with reconstruction of the history of ocean/climate interactions by means of high-resolution palaeoceanographic records. IMAGES cruise *Marion Dufresne 101* in 1995 (Bassinot & Labeyrie 1996) cored on the Iberian margin, because the rapidly accumulated sediments there lie at a sensitive latitude with respect to the different surface ocean temperature fields which develop during glacial and interglacial times. The Polar Front progressively retreats counterclockwise during deglaciation, from an approximate east–west orientation as far south as 40°N during glacial maximum times (CLIMAP 1976), to its present more northerly interglacial NW–SE orientation along the eastern Canadian seaboard. The rate of change on this margin is particularly dramatic in the early stages of deglaciation (Ruddiman & McIntyre 1981). Sediments of the Iberian margin also contain evidence of ice-rafted materials from Heinrich Events, the short-duration episodes of iceberg releases from high Atlantic latitudes which occur during glacial periods (Kudrass 1973; Lebreiro *et al.* 1996; Baas *et al.* 1997; Zahn *et al.* 1997).

The micropalaeontology of the changes in surface ocean productivity of the Iberian margin has been described by Abrantes and co-workers (Abrantes 1988, 1990; Lebreiro *et al.* 1997; Abrantes *et al.* 1998). The sedimentology of the recent deposits of the Iberian shelf and slope has recently been reviewed and interpreted by Baas *et al.* (1997) and Zahn *et al.*

(1997), while Thomson *et al.* (1999) have examined the changing accumulation rate fluxes through the last two glacial/interglacial transitions (0–150 ka). In this paper, a good chronostratigraphic model is developed for a 35 m core from the mid-slope, and the geochemical and micropalaeontological palaeoproductivity indicators in the core are examined.

Material and methods

Core MD95-2039 is a 35 m *Calypso* giant piston core collected to the west of Oporto Seamount in 3381 m water depth by *RV Marion Dufresne* in 1995 (Bassinot & Labeyrie 1996; Fig. 1). The core was sampled at 10 cm spacing for most analyses. For the SOC geochemical analyses, volume-defined samples were oven-dried at 100°C and ground for analysis in a tungsten carbide swing mill mortar. Calcium carbonate and C_{org} were determined on all samples by coulometry, with $CaCO_3$ measured from the CO_2 liberated by 10% phosphoric acid, and C_{org} by subtraction of $CaCO_3$-derived CO_2 from the CO_2 liberated on whole sample combustion at 900°C. The bulk sediment compositions of a sub-set of samples were determined for selected major and trace elements (Al, Si, Ca, Mg, Ba, Zr and Cr) by simultaneous inductively coupled plasma atomic emission spectrometry (ICP-AES), after total sample dissolution effected by lithium metaborate fusion (Jarvis 1992).

For the sedimentological and isotopic studies undertaken at GEOMAR, volume-defined sub-samples of 15–25 cm³ were taken at the same levels as the samples used by SOC. All samples were frozen at −40°C, dried *in vacuo*, soaked with water until disintegration, washed through a 63 µm mesh screen, and dried. Stable isotope
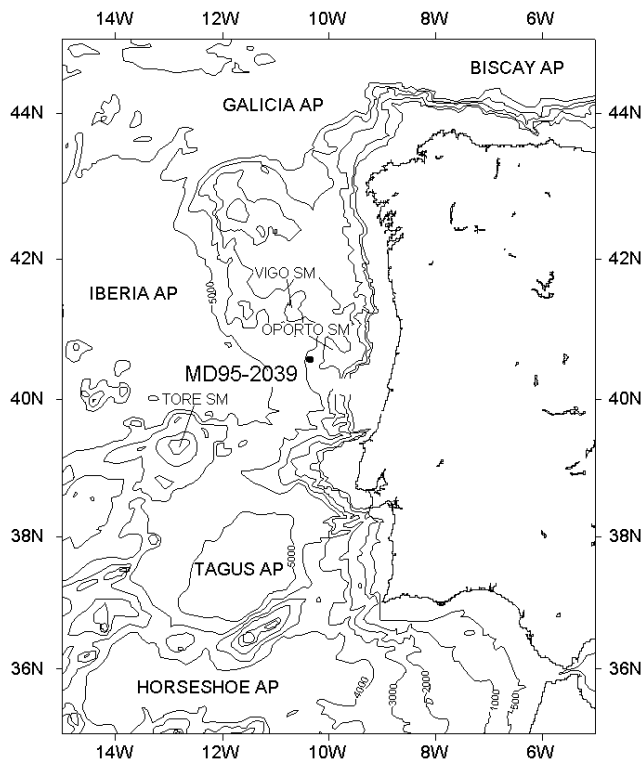
Fig. 1. Location of core 2039 on the Portuguese margin.

Fig. 2. $\delta^{18}O$ isotope record of $>250\,\mu m$ fraction benthic foraminifera *Cibicidoides wuellerstorfi* (0–3520 cm) and *Uvigerina pygmea* (3530–3570 cm; -0.64% for conversion to *Cibicidoides* scale), $>63\,\mu m$ bulk coarse fraction and ages of inferred chronostratigraphic points, all as a function of depth in core MD95-2039. Note that $\delta^{18}O$ values are presented $\times -1$. Open circles are *calibrated radiocarbon ages* (see text), closed circles are Heinrich Event maxima, small filled squares are oxygen isotope in-stage events and large filled squares are oxygen isotope stage boundaries. Oxygen isotope stages 1, 3, 5, 7 and 9 are shaded. The dashed lines indicate the mean sediment accumulation rates before and after the oxygen isotope stage 5/4 boundary, 7.5 and 21 cm ka^{-1}, respectively. The sharp change in mean accumulation rate at 15.5 m (right panel) may be caused by a corer artefact.

measurements were run on 1–11 well-preserved specimens picked from the $>250\,\mu m$ size fraction of the benthic foraminifers *Cibicidoides wuellerstorfi* (0–3530 cm) and *Uvigerina pygmea* (3530–3570 cm). The tests were ultrasonically rinsed in methanol to remove surface contamination. Isotope analyses were made with an on-line carbonate preparation line (Carbo-Kiel—single sample acid bath) connected to a Finnigan Mat 252 mass spectrometer at the Institute of Geology and Mineralogy, University of Erlangen, Germany. Isotope data are reported in per mille relative to PDB by assigning a $\delta^{13}C$ and $\delta^{18}O$ values of $+1.95$ and -2.20, respectively, to the standard NBS19. The external reproducibility of the measurements is $\pm 0.2\%$ for $\delta^{13}C$ and $\pm 0.3\%$ for $\delta^{18}O$ as calculated from replicate analyses of the internal carbonate standard (Solnhofen limestone) and NBS 19 over 1 hour. The precision ranges from ± 0.01 to ± 0.06 (stdv) for both $\delta^{13}C$ and $\delta^{18}O$.

At IGM-DGM Lisbon, untreated bulk sediment, sampled at 10 cm spacing, was used to prepare the smear slides used in diatom quantification, and diatom abundance was estimated as the percentage of the total area of observation occupied by diatoms. The dolomite content was determined by a combination of X-ray diffraction and the gasometric method of Hulsemann (1966) (Gaspar *et al.* 1996).

Additional 50 cm^3 samples for ^{14}C age determination were taken at the core repository. Thirteen monospecific samples of planktic foraminifera were analysed, nine comprising 275–1529 *Globigerina bulloides* tests from the $>250\,\mu m$ size fraction, and four comprising 1464–1648 tests of *Neogloboquadrina pachyderma* (sin) from the 150–250 μm size fraction. All samples were ultrasonically rinsed in methanol, and treated with 10% H_2O_2 and dilute HCl to remove organic material and carbonate dust before analysis. Radiocarbon ages were determined via accelerator mass spectrometry (AMS) using the 3MV Tandetron system at the Leibniz-Labor of Kiel University (Nadeau *et al.* 1997; Table 1).

It has been found by N. Thouveny (CEREGE, Europole de l'Arbois BP 80, 13545 Aix en Provence, France) that the upper 10–15 m of some Calypso cores appear longer by a factor of 1.5–2 than comparative conventional piston cores. This difference does not arise from a simple stretching of the sediment section, but involves some syringing

or over-sampling of the sediments and a microfabric rotation into the vertical. This corer artefact is now suspected as the cause of the apparent abrupt accumulation rate change at 15 m depth in core MD95-2039 (Fig. 2). Despite this artefact, however, the recovered stratigraphies of Calypso cores appear true even at a centimetric scale (N. Thouveny, pers. comm. 1999). In this paper, such an effect will affect accumulation rate estimates but not other interpretations.

Results and discussion

Chronostratigraphy of core MD95-2039

Establishment of a chronological framework for core MD95-2039 is necessary before productivity signals can be interpreted. Over the past 40 ka, the conversion from depth in core to time can be achieved by means of the planktonic foraminifera radiocarbon ages (Table 1) and the depths at which the most recent Heinrich Events occur. At times >40 ka, a time-scale is derived by matching the known times of characteristic peaks, troughs and transitions in the oxygen isotope stages in the $\delta^{18}O$ record of benthic foraminifer *Cibicidoides wuellerstorfi* (Table 2).

In discussion we distinguish between *radiocarbon convention ages* and *calibrated radiocarbon ages*. Radiocarbon convention ages are the analyses reported according to the Stuiver & Polach (1977) protocol (Table 1). Such ages require a reservoir

Table 1. *Radiocarbon ages determined for planktonic foraminifers* Globigerina bulloides *and* Neogloboquadrina pachyderma

Laboratory no.	Depth (cm)	Planktonic species	Radiocarbon convention age (years)	Error +1σ (years)	Error −1σ (years)	Corrected C-14 age (ka)
KIA779	38.5	G.b.	6150	50	50	6.32
KIA780	168.5	G.b.	12 620	110	110	13.73
KIA781	208.5	G.b.	13 520	100	100	14.89
KIA782	208.5	N.p.	13 930	100	100	
KIA783	288.5	G.b.	14 250	110	110	15.75
KIA784	288.5	N.p.	14 650	110	110	
KIA785	542.5	G.b.	20 140	210	200	23.33
KIA786	542.5	N.p.	20 720	220	210	
KIA787	648.0	G.b.	22 810	280	270	25.73
KIA788	818.5	G.b.	27 980	520	490	31.02
KIA789	949.0	G.b.	29 000	590	550	(31.95)
KIA790	1019.0	G.b.	30 130	690	640	(33.62)
KIA791	1019.0	N.p.	31 950	860	770	

*Radiocarbon convention age, − 400 years for surface ocean reservoir age, and corrected according to Laj *et al.* (1996).
Ages in parenthesis appear too young and were not included in the chronostratigraphic model.
Globigerina bulloides (G.b.; >250 μm in size) and *Neogloboquadrina pachyderma* (N.b.; 150–250 μm).

modification of − 400 years to correct for the surface ocean and atmospheric age difference (Bard 1988). Reservoir-corrected radiocarbon convention ages were then further corrected to calibrated radiocarbon ages (Tables 1 and 2) by application of the model correction of Laj *et al.* (1996). Direct empirical relationships for radiocarbon ages are available only back to 20 ka (Bard *et al.* 1993). The Laj *et al.* (1996) correction is derived from modelling the coupling of ^{14}C production in the atmosphere to the earth's geomagnetic field intensity and an ocean circulation change effect, and applies over the past 50 ka.

The magnetic susceptibility record of the core measured on retrieval (Bassinot & Labeyrie 1996; not shown) displayed discrete maxima, the upper five of which coincide with peaks in the >63 μm coarse-fraction record (Fig. 2). These coincident susceptibility and coarse fraction maxima represent the enhanced ice-rafted detrital (IRD) inputs transported by Heinrich Events (Jung 1996). The depths of these Heinrich Events levels provide chronostratigraphic points for the upper core, because the times of the most recent Heinrich Events have now been estimated in cores from a wide North Atlantic area (Bond *et al.* 1992, 1993; Manighetti *et al.* 1995; Lebriero *et al.* 1996; Cortijo *et al.* 1997; Vidal *et al.* 1997; Zahn *et al.* 1997).

The paired radiocarbon convention ages from the species separates of the same four samples in the upper section of core MD95-2039 are consistently higher for the *N. pachyderma* (sin.) analyses than for the corresponding *G. bulloides* analyses (Table 1). The *N. pachyderma* (sin.) samples were from a smaller size fraction, 150–250 μm compared to >250 μm for *G. bulloides*, so that contamination of the *N. pachyderma* ages by redeposited small shells cannot be excluded (Lutze *et al.* 1979). Systematic and differential size-related bioturbation, or offsets in abundance peaks of the two species, are further possibilities which may account for these age differences (e.g. Thomson *et al.* 1995*b*; Manighetti *et al.* 1995; Trauth & Sarnthein 1997). The means of these paired calibrated radiocarbon ages were used to confirm the chronology for the upper part of core (Tables 1 and 2).

The interpolated radiocarbon convention ages for Heinrich Events H1, H2 and H3 are reasonably close to those determined previously (Bond *et al.* 1992, 1993; Manighetti *et al.* 1995; Lebreiro *et al.* 1996; Vidal *et al.* 1997; Zahn *et al.* 1997). There is little doubt in the identification of H4 at 1020 cm, because this is the largest Heinrich Event in this part of the Atlantic (Lebreiro *et al.* 1996; Zahn *et al.* 1997). The radiocarbon convention age of 30.64 ka near H4, however, is much younger than both the 36.1 ka estimated by interpolation in the Iberian slope core SO75-26KL (Zahn *et al.* 1997) and the 33.2–35.1 ka from more northerly Atlantic cores (Cortijo *et al.* 1997). It is difficult to define the source of this apparent shift of *c.* 5 ka towards young ages, but possibilities include trace contamination of such old foraminiferal samples (e.g. by carbonate dust or tap-water bicarbonate during sample preparation). To ensure stratigraphic comparability with other North Atlantic core records, the radiocarbon convention ages of samples KIA 789 and 790/1 are disregarded.

The radiocarbon convention ages given by Zahn *et al.* (1997) for Heinrich Events 1 and 2 are used because they are based on a series of closely-spaced radiocarbon ages. The radiocarbon convention age for H3 is taken from Bond *et al.* (1992) who reported ages immediately above and below the H3 horizon. For H4, the radiocarbon convention age of Cortijo *et al.* (1997) was used, and for H5 the estimate of Kiefer (1998). The age of H6 has been estimated at 66 ka (Bond *et al.* 1993) and should occur in early stage 4 between the oxygen isotope events 4.22 and 4.23 of Martinson *et al.* (1987). There is a gap in the susceptibility record of core MD95-2039 around this level, but a small coarse fraction peak does occur at 1460 cm which is tentatively assigned to H6 (Table 2). Our adopted estimates for times of emplacement of Heinrich Events are all somewhat younger than those of Manighetti *et al.* (1995), possibly because of differential bioturbation effects at the relatively low sedimentation rates encountered in their NE Atlantic cores.

Correlations from core MD95-2039 to the earlier H7-H11 defined by Heinrich (1988) in cores from the Northeast Atlantic Dreizack Seamount area are less certain than for the

Table 2. *Chronostratigraphic model for core MD95-2039 using Heinrich Events (HE), oxygen isotopic stage (OIS) depths and corrected radiocarbon ages*

Event (OIS or HE) or radiocarbon analysis no.	Depth in MD95-2039 (cm)	Age assigned (ka)	Source reference	Convention age used (ka, − 400 a res. correct.)	Calibrated age used (ka)
Core top	2	—	—	—	0
KIA 779	38.5	—	—	5.75	6.32
1.1	100	9.10	Winn *et al.* (1991)	9.10	10.10
(2.0)	(130)	—	—	—	—
KIA 780	168.5	—	—	12.22	13.73
KIA 781/2	208.5	—	—	13.33	14.89
H1	214	13.54	Zahn *et al.* (1997)	13.54	15.12
KIA 783/4	288.5	—	—	14.05	15.75
(3.0)	(490)	—	—	—	—
KIA 785/6	542.5	—	—	20.03	23.33
H2	544	20.46	Zahn *et al.* (1997)	20.46	23.78
KIA 787	648	—	—	22.41	25.73
H3	768	27.00	Bond *et al.* (1993)	27.00	30.46
KIA 788	818.5	—	—	27.58	31.02
KIA 789	949	—	—	(28.60)	(31.95)
KIA 790/1	1019	—	—	(30.64)	(33.62)
H4	1020	34.15	Cortijo *et al.* (1997)	34.15	36.96
3.13	1185	42.00	Zahn *et al.* (1997)	42.00	43.88
H5	1216	45.80	Kiefer (1998)	—	45.80
3.3	1295	50.21	Martinson *et al.* (1987)	—	50.21
3.31	1360	55.45	Martinson *et al.* (1987)	—	55.45
4.0	1415	58.69	Martinson *et al.* (1987)	—	58.69
(H6)	(1460)	—	—	—	—
5.0	1550	73.91	Martinson *et al.* (1987)	—	73.91
5.1	1660	79.25	Martinson *et al.* (1987)	—	79.25
5.2	1710	90.95	Martinson *et al.* (1987)	—	90.95
5.3	1760	99.38	Martinson *et al.* (1987)	—	99.38
5.4	1850	110.79	Martinson *et al.* (1987)	—	110.79
5.5	1900	123.82	Martinson *et al.* (1987)	—	123.82
6.0	1970	129.84	Martinson *et al.* (1987)	—	129.84
6.2	2030	135.10	Martinson *et al.* (1987)	—	135.10
6.3	2230	142.28	Martinson *et al.* (1987)	—	142.28
6.4	2300	152.58	Martinson *et al.* (1987)	—	152.58
6.41	2330	161.34	Martinson *et al.* (1987)	—	161.34
6.42	2365	165.35	Martinson *et al.* (1987)	—	165.35
6.5	2402	175.05	Martinson *et al.* (1987)	—	175.05
6.6	2510	183.30	Martinson *et al.* (1987)	—	183.30
7.0	2540	189.61	Martinson *et al.* (1987)	—	189.61
7.1	2600	193.07	Martinson *et al.* (1987)	—	193.07
7.2	2620	200.57	Martinson *et al.* (1987)	—	200.57
7.3	2660	215.54	Martinson *et al.* (1987)	—	215.54
7.4	2740	224.89	Martinson *et al.* (1987)	—	224.89
7.5	2790	240.19	Martinson *et al.* 1987)	—	240.19
8.0	2810	244.18	Martinson *et al.* (1987)	—	244.18
8.2	2900	249.00	Imbrie *et al.* (1984)	—	249.00
8.3	2980	257.00	Imbrie *et al.* (1984)	—	257.00
8.4	3110	265.67	Martinson *et al.* (1987)	—	265.67
8.5	3240	288.54	Martinson *et al.* (1987)	—	288.54
8.6	3320	299.00	Imbrie *et al.* (1984)	—	299.00
9.0	3340	303.00	Imbrie *et al.* (1984)	—	303.00
9.1	3380	310.00	Imbrie *et al.* (1984)	—	310.00
9.2	3470	320.00	Imbrie *et al.* (1984)	—	320.00
9.3	3520	331.00	Imbrie *et al.* (1984)	—	331.00
10.0	3560	339.00	Imbrie *et al.* (1984)	—	339.00

Note: Depths or times in parenthesis were not used in the age to time conversion.

more recent Heinrich Events. During oxygen isotope stage 5, two magnetic susceptibility maxima occur at 1640 and 1750 cm, but these correspond to minima in the $CaCO_3$ record rather than the >63 μm coarse fraction peaks also found in oxygen isotope stage 5. The benthic (*Pyrgo murrhina*) and planktonic (*G. bulloides*) oxygen isotope records from core Me69-17 used by Heinrich (1988) do not resolve isotope stages 5.1 through 5.4 sufficiently well to allow a detailed comparison between Heinrich's IRD and foraminiferal faunal peaks with the oxygen isotope stage 5
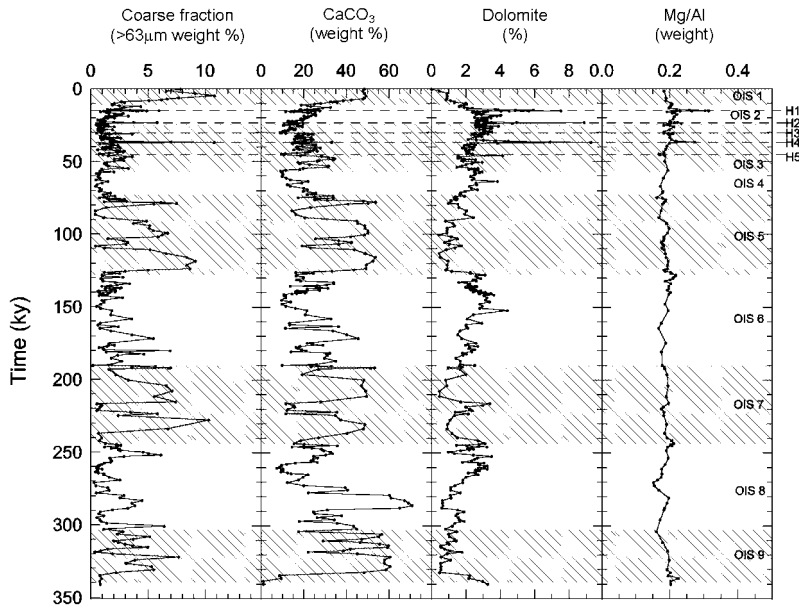
Fig. 3. Concentration versus time profiles of >63 μm bulk coarse fraction, $CaCO_3$ wt%, dolomite wt% and Mg/Al mass ratio in core MD95-2039. Oxygen isotope stages 1, 3, 5, 7 and 9 are shaded, and positions of Heinrich Events H1–H5 are indicated by dashed lines. The presence of dolomite increases the Mg/Al ratio of *c.* 0.2 typical of the clay/$CaCO_3$ mix of the sediments accumulated outside Heinrich Events.

record of core MD95-2039. The warmer sub-stages 5a, 5c and 5e and the colder stages 5b and 5d are very clearly resolved in core MD95-2039, however, so that over this core section preference was given to ages of oxygen isotope events as the chronostratigraphic points for the age model (Table 2, Fig. 2).

The major features of the oxygen isotope record of core MD95-2039 can readily be reconciled with the generalized SPECMAP curve of Imbrie *et al.* (1984) and the core records of Martinson *et al.* (1987) and Bassinot *et al.* (1994). The work of Bassinot *et al.* (1994) represented a marked improvement in the nomenclature and dating of oxygen isotope events earlier than the 9/10 stage boundary, but this is the earliest datum recognized in core MD952039. The differences in the ages for isotopic events later than the 9/10 stage boundary determined by Bassinot *et al.* (1994) and earlier estimates (Imbrie *et al.* 1984; Martinson *et al.* 1987) are ± <5 ka. Martinson *et al.* (1987) used a broader, globally distributed data set of seven stacked benthic isotope curves (Pisias *et al.* 1984) as the target curve for their tuning procedure, and their scheme also allows the recognition of various sub-events. The timescale of Martinson *et al.* (1987) was therefore applied for the middle part of the core MD95-2039 and that of Imbrie *et al.* (1984) in the lower part (Table 2).

According to the oxygen isotope stratigraphy, the stage 10/9 boundary at 339 ka occurs in core MD95-2039 at 3560 cm, just above the base of the core at 3570 cm (Fig. 2). The mean whole-core sediment accumulation rate for MD95-2039 is therefore 10.4 cm ka^{-1}, with a maximum rate of 38 cm ka^{-1} occurring between H1 and H2. When the full time/depth curve (Fig. 2) is examined, a change in long-term mean accumulation rate is evident at the oxygen isotope stage 5/4 boundary at 1560 cm or 73.91 ka (dotted lines in Fig. 2). Above this boundary to the core top the mean accumulation rate is 21 cm ka^{-1}, whereas between the oxygen isotope stage 10/9 and 5/4 boundaries the mean rate is 7.5 cm ka^{-1}. Within this broad picture, the actual rates within the glacial oxygen isotope stages 6 and 8 are slightly more rapid than within the warmer oxygen isotope stages 5 and 7, as judged from the local slopes of the line connecting the time/depth data within the oxygen

isotope stages. Potential over-sampling by the Calypso corer means that the high apparent accumulation rates calculated for the upper 1560 cm of the core must now be treated with some caution. This corer sampling artefact is currently under investigation, and at present the only technique to quantify the necessary correction is a direct comparison with a core at the same location from another type of corer (N. Thouveny, pers. comm. 1999).

Heinrich Events

The most recent Heinrich Event layers in core MD95-2039 were identified above as H1-H5. Although the contribution of exotic ice-rafted material by Heinrich Events to the total sediment accumulation flux is small at this latitude (Thomson *et al.* 1999) by comparison with the high IRD flux latitudes further north (Grousset *et al.* 1993), these Heinrich Events are revealed as distinct peaks in the >63 μm coarse fraction percentage profile over the last glacial (oxygen isotope stages 2, 3 and 4) sediment background values of <3% (Fig. 3). Note, however, that earlier coarse fraction peaks of a similar, or even larger, magnitude than those of recent Heinrich Events also occur during interglacials (odd-numbered oxygen isotope stages). These interglacial coarse fraction maxima coincide with high interglacial carbonate contents, and are caused by an increase in the relative abundance of (planktonic) foraminifera in the slower-accumulated interglacial marls (>30% $CaCO_3$) compared with the glacial clays (<30% $CaCO_3$; Fig. 3).

For H1, H2 and H4, where the ice-rafted material is particularly abundant, the exotic mineralogy of the sediments is also revealed by local increases in dolomite content and in whole-sediment Mg/Al ratios (note that the Mg/Al data are at a lower sampling resolution than the XRD data). Dolomite does not occur in all Heinrich Events (Thomson *et al.* 1995a; Lebreiro *et al.* 1996; Gaspar *et al.* 1996), but the XRD technique clearly has an excellent sensitivity for this sub-set of Heinrich Events (Fig. 3). The XRD data for the H2 level indicates a different clay mineralogy with a higher kaolinite content, which may be the reason for the difference in the
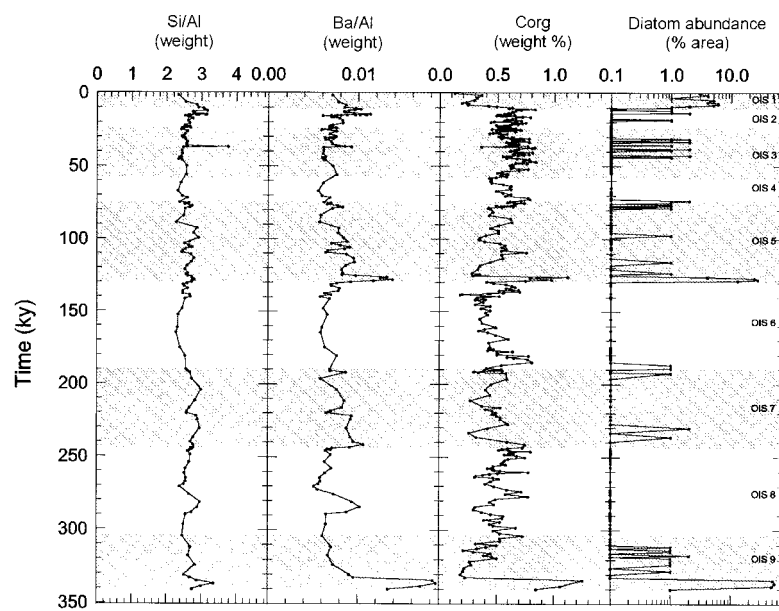
Fig. 4. Concentration versus time profiles of C_{org} wt%, diatoms (% area of observation, note logarithmic scale), Ba/Al mass ratio and Si/Al mass ratio in core 2039. Oxygen isotope stages 1, 3, 5, 7 and 9 are shaded.

signal magnitudes of the dolomite and the Mg/Al records in this case.

XRD also reveals that glacial sediments of oxygen isotope stages 2, 3, 4, 6 and 8 have greater background dolomite contents than during interglacial periods. It is not clear whether this dolomite is introduced solely by some combination of ice rafting and currents during glacial stages, or whether there is also a diagenetic contribution (Gaspar *et al.* 1996). The dolomite content increases upwards in glacial oxygen isotope stages 8 and 6 as it does through the stage 4, 3 and 2 combination, but the criteria used to identify earlier Heinrich Events (high coarse fraction percentages, high dolomite contents and distinct spikes in the magnetic susceptibility record) fail to identify Heinrich Events older than 75 ka. Further north, Van Krefeld *et al.* (1996) reported IRD accumulation rates for Heinrich Events older than H6 which are less than a half of those estimated for H1–H5. The pattern of North Atlantic ice-rafting changed dramatically around *c.* 75 ka, with meridional IRD maxima along the Greenland-Newfoundland coasts during all of oxygen isotope stage 5, but with an axis after that time during oxygen isotope stages 2, 3 and 4 further south at 40–50°N (Ruddiman 1977). This latter axis is the Heinrich Event zone of Grousset *et al.* (1993). This observation was ascribed by Ruddiman (1977) to different cyclonic flow patterns of the sub-polar gyre, and he envisaged that similar shifts would be repeated in earlier glacial/interglacial cycles. The data from core MD95-2039 do not in fact suggest that Heinrich Event ice-rafting did persist as far south as the Iberian margin during glacial stages in the 75–350 ka period, in contrast to the several Heinrich Event occurrences recorded during the last glacial stage. The other possibility is that any such earlier events have been entirely missed in MD95-2039 because of lower sampling resolution, a possibility which arises from the combination of fixed sampling interval and the sharp decrease in apparent accumulation rates earlier than the 5/4 boundary (Fig. 2).

Local increases in Ba/Al and Si/Al ratio profiles occur along with dolomite and Mg/Al at the levels of the largest Heinrich Events, H1, H2 and H4. As Ba/Al will be used later to assist identification of palaeoproductivity pulses (Fig. 4), the question arises whether the Heinrich Events are accompanied by high productivity, or whether peaks in the Ba/Si and Si/Al ratios represent a primary compositional difference in the sediments containing Heinrich Events, like Mg/Al, or whether they are related to productivity changes. Major diatom spikes associated with Heinrich Events have been found in a core from the Azores basin (Kiefer *et al.* 1995). Planktonic foraminifera data from the Iberian Basin off Portugal (Lebreiro *et al.* 1997; Abrantes *et al.* 1998) also indicate marked surface productivity and export production increases associated with Heinrich Events. Nevertheless it appears most likely that the Ba/Al and Si/Al ratios in core MD95-2039 represent primary compositional differences, on the evidence that there is no corresponding increase in diatom or C_{org} contents at these levels.

The compositional and productivity record of core MD95-2039

The flux of C_{org} to sediments is expected to be proportional to surface ocean productivity, and various algorithms are available to estimate palaeoproductivity from sediment C_{org} content (e.g. Betzer *et al.* 1984; Sarnthein *et al.* 1992). Other biologically derived components, such as biogenic $CaCO_3$ (Brummer & van Eijden 1992) and opal (Shrader & Sorkness 1991) can also respond similarly to C_{org} production, and are therefore often used as proxies along with, or instead of, C_{org} contents to identify high productivity episodes. Just as the C_{org} signal recorded in sediments is degraded by post-depositional remineralization in oxic and anoxic conditions after deposition, however, these proxy parameters also have a variable post-depositional preservation.

Calcium carbonate records

The different accumulation rates through glacial and interglacial times in core MD95-2039 result in changes in bulk sediment composition, particularly in $CaCO_3$ content (Fig. 3). Over the full 350 ka record of the core (mean $CaCO_3$ content=26%; Fig. 3), maximum $CaCO_3$ contents tend to be found as well-organized peaks within the sediments of interglacial oxygen isotope stages 1, 5, 7 and 9, which also tend to

be coincident with lowest $\delta^{18}O$ values. Glacial sediments generally have lower $CaCO_3$ values, although there are pulses of high $CaCO_3$ content in the sediments of oxygen isotope stages 6 and 8, the latter of which represents the maximum $CaCO_3$ value in the entire core (71%). The case has been made from sediment trap studies that present-day $CaCO_3$ flux is linearly related to C_{org} productivity flux (Brummer & van Eijden 1992), and core $CaCO_3$ data have been used to deduce palaeoproductivities (e.g. van Kreveld *et al.* 1996).

When the calcium carbonate content profile of core MD95-2039 is analysed statistically as a function of time, significant periodicites of 18.8, 23.7, 38.0 and 100.6 ka are found in the record (see Fig. 5 caption for method). The first two of these frequencies correspond to those of the earth's orbital precession, the third to that of orbital obliquity and the fourth to that of orbital eccentricity (Berger & Loutre 1991). Note that theoretical mean values for the orbital frequencies (19, 23, 41 and 100 ka) have been combined in Fig. 5 to reproduce a shape similar to that of the core MD95-2039 carbonate content curve, rather than the (similar) empirical values quoted above. There is some circularity involved in the procedure adopted to mimic the $CaCO_3$ record in Fig. 5 because the time-scale of the carbonate record was derived via the marine $\delta^{18}O$ curve, the chronology of which has been tuned through the assumption that the oxygen isotope record responds to orbital frequencies (Imbrie *et al.* 1984, 1992). The fact that these Milankovitch frequencies are also present in the $CaCO_3$ record of the core, however, indicates that the carbonate content of the sediments in this area respond to orbital forcing frequencies as well as the $\delta^{18}O$ record. This control on carbonate content cannot be ascribed to carbonate productivity changes, however. Over the 140 ka for which $(^{230}Th_{excess})_0$ data were available, Thomson *et al.* (1999) demonstrated that the primary control on the changing $CaCO_3$ contents in this core was clay flux variation rather than carbonate productivity variation. Over the analysed 0–140 ka section, the mean regional $CaCO_3$ flux was 0.91 ± 0.83 g cm^{-2} ka^{-1} whereas the mean regional clay flux was 3.05 ± 1.73 g cm^{-2} ka^{-1}, and to a first approximation the $CaCO_3$ contents of the core represent a blend of a fairly constant $CaCO_3$ flux dominated by a more variable clay flux. This clay flux is governed by sea level, with highest clay fluxes at times of lowest sea level and vice versa. This is a consequence of the trapping of river-derived clays on the continental shelf during interglacial times with high sea level, whereas sediment is supplied to the deep sea and submarine fans only during glacial periods when enhanced ice volume draws down sea level (Gibbs 1981; Bacon 1984; McManus *et al.* 1998). The orbital periodicities observed in the $CaCO_3$ record (Fig. 5) must therefore be controlled primarily by clay flux dilution cycles rather than $CaCO_3$ productivity flux cycles.

Barium as a palaeoproductivity indicator

The contents of other compositional species (e.g. clay, defined as $[1 - CaCO_3\%/100]$) are directly affected by $CaCO_3$ content fluctuations because of the closed sum effect (Rollinson 1993). For elements expected to be primarily associated with the clay or detrital phase, the closed sum problem is treated here by normalizing the elemental data to Al content (e.g. Ba/Al).

Enhanced concentrations of the element Ba have long been recognized to accompany high productivity (e.g. Goldberg & Arrhenius 1958), so that Ba is regularly used as a palaeo-productivity indicator. Settling material from surface ocean
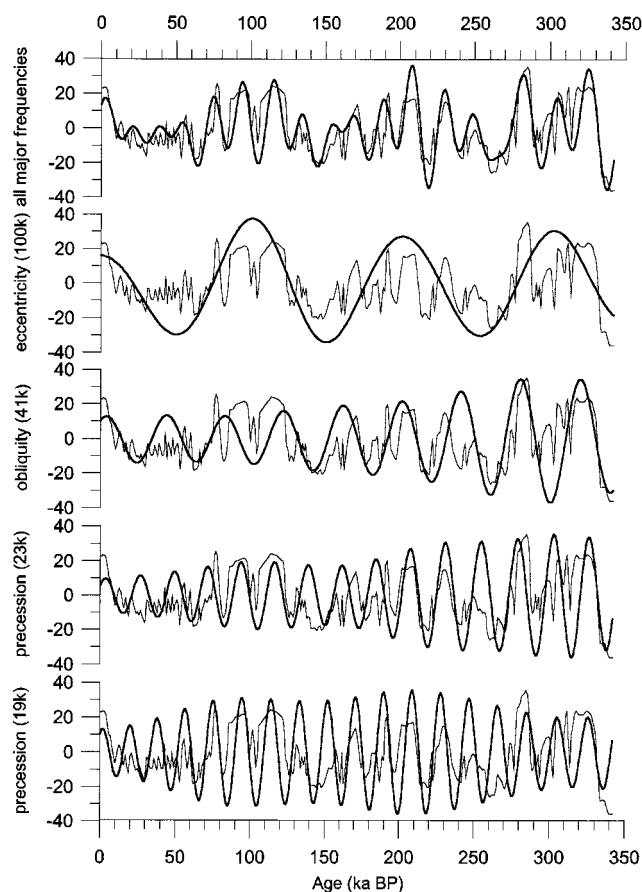
Fig. 5. Milankovitch frequencies in the MD95-2039 $CaCO_3$ record. This figure is the result of the following stages of analysis. (i) The $CaCO_3$ data as a function of age (Fig. 3) were linearly interpolated and read in 1 ka steps. The equally-spaced record was then detrended by subtraction of a least squares linear fit through the data, and the residual record normalized to mean=0. No further smoothing was applied to the residual record before analysis. (ii) The power spectrum of the residual record was calculated by autocorrelation over N/4 lags, and spectral values calculated from the autocorrelation matrix by means of a complex Fourier transformation. The result was expressed in terms of variance density (spectral value divided by frequency). The $\log_{10}$(variance density) data versus frequency were then smoothed once with a Hanning filter. The background spectrum was determined by a quadratic fit through the variance density values and 80, 90 and 95% confidence intervals assessed according to χ^2 distribution values. (iii) The main frequencies present above the 90% confidence interval in the MD95-2039 $CaCO_3$ record indicated periodicities of 18.8, 23.7, 38.0 and 100.6 ka, which closely match Berger & Loutre's (1991) values for the earth's orbital periods of eccentricity (404, 123.8 and 94.8 ka), obliquity (41.1 ka) and precession (23.7, 22.4 and 19.0 ka). (iv) The residual (detrended) record versus age was analysed using Blackman band pass filters representative of the 19, 23, 41 and 100 ka periodicities with bandwidths of $\pm 10\%$. In this figure the four individual results are presented in the lower four panels, each superimposed on the residual record and scaled so that the filtered components have similar maximum amplitudes to the record. In the top panel, the filtered components are added and the cumulative signal is scaled to, and plotted over, the residual record.

organic productivity develops a Ba enrichment as biogenic barite during its descent through the water column before deposition (Bishop 1988), and there are similarities between
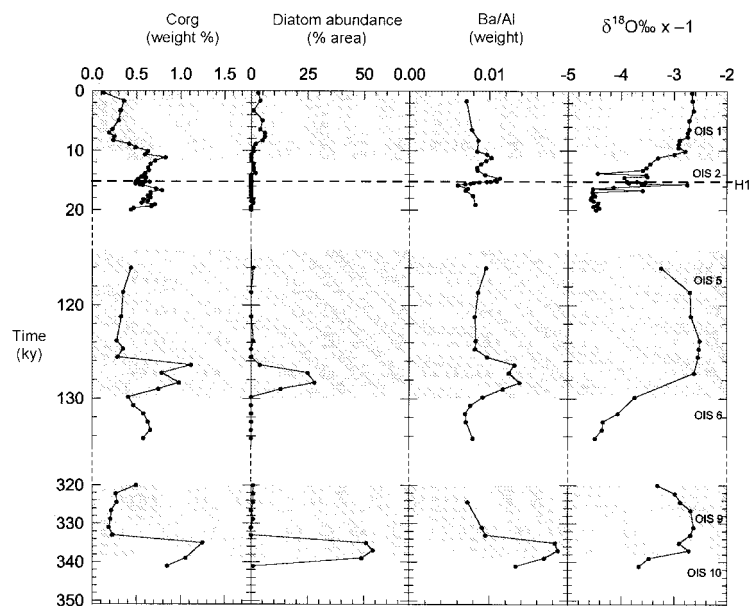
Fig. 6. Detail of the concentration versus time profiles of C_{org} wt%, diatoms (% area of observation), Ba/Al mass ratio and Si/Al mass ratio in core MD95-2039 at the oxygen isotope stage 10/9, 6/5 and 2/1 boundaries. These three boundaries mark the abrupt changes from maximal full glacial to full interglacial conditions and the largest sea level rises during the period covered by this core (Shackleton 1987; Rohling *et al.* 1998).

the biological Si and Ba cycles in the ocean (Chan *et al.* 1976). At times of high productivity, the flux of biogenic Ba becomes sufficiently large to be readily identified against the detrital Ba level in the sediments through increases in the total sediment Ba/Al ratio. Despite intensive recent investigation (Dymond *et al.* 1992; Dymond & Collier 1996), the mechanisms by which the $Ba_{biogenic}/C_{org}$ ratio is set in new marine productivity, and the modifications to the $Ba_{biogenic}/C_{org}$ ratio during settling through the water column, remain unclear. As a result, it is not yet been possible to refine a quantitative relationship between Ba and C_{org} settling fluxes (Dymond & Collier 1996). Further modification of the $Ba_{biogenic}/C_{org}$ ratio occurs during C_{org} remineralization in sediments, and another complication occurs within the sediments when reduction draws SO_4^{2-} pore water concentrations below the barite solubility product level. Dissolved Ba^{2+} from barite then diffuses upwards to form diagenetic barite peaks higher in the sediment section where higher SO_4^{2-} pore water levels exceeding the barite solubility product level are still found (Brumsack 1986; Torres *et al.* 1996). A knowledge of the pore water geochemistry with depth is required to differentiate the diagenetic barite peaks which can result from this process from the biogenic barite peaks related to productivity pulses.

In core MD95-2039, the largest C_{org}, Ba/Al and diatom peaks are all coincident with the upper part of the oxygen isotope stage 10/9 transition, and the second largest peaks are on the upper part of the oxygen isotope stage 6/5 transition (Fig. 4). Over the period encompassed by this core, the 1/2, 5/6 and 9/10 oxygen isotope transitions mark the most abrupt changes from maximal full glacial to full interglacial conditions and the associated largest sea level rises (Shackleton 1987). These oxygen isotope transitions are sometimes named Terminations I, II and IV, respectively (Broecker & van Donk 1970). The 8/7 oxygen isotope transition (Termination III) was smaller and more gradual than these other transitions (Shackleton 1987; Rohling *et al.* 1998). Although the C_{org} and Ba/Al peaks at the oxygen isotope stage 2/1 transition are not as prominent as those at the 5/6 and 9/10 transitions, both are at relatively high values in their whole-core records but do not have an associated diatom maximum (Figs 4 and 6).

Apparently similar productivity signals, involving simultaneous Ba and other productivity proxy maxima, have been recognized at one or more glacial/interglacial transitions in the NW African upwelling area. Harris *et al.* (1996) found such signals at the 10/9 and 6/5 transitions, and they are also evident at the 6/5 transition in the shorter record of Matthewson *et al.* (1995). Local Ba peaks have also recently been reported in the sediments of glacial terminations in several other Atlantic localities by Kasten *et al.* (1997). Some of these localities are currently relatively oligotrophic (western and eastern equatorial Atlantic Ocean, Ceara and Sierra Leone Rises). These Ba maxima have been ascribed by Kasten *et al.* (1997) to diagenetic processes rather than to productivity, on the basis of (i) a lack of correlation with any other productivity indicator and (ii) associations of Ba with other redox-sensitive elements. It therefore remains to be established if a single explanation is applicable to all Ba peaks found at glacial/interglacial transitions. It is possible that, in different circumstances, they may arise either from short-duration high productivity episodes, or alternatively from diagenesis in the sediments as a result of re-adjustments in sediment geochemistry between glacial and interglacial periods (Torres *et al.* 1996). The explanation preferred by Kasten *et al.* (1997) is inconsistent with both the core MD95-2039 and NW African evidence cited above, however, where the enhanced Ba is clearly coincident with both enhanced C_{org} contents and diatom abundances.

Diatoms as a palaeoproductivity indicator

High diatom abundance in sediments has long been used as a palaeoproductivity indicator (e.g. Kanaya 1966; Donahue 1970; Maynard 1976; Sancetta 1979; Barde 1981). Diatoms mainly of the genus *Chaetoceros Ehrenberg* are known to dominate the phytoplankton of upwelling areas, and its presence in export production is confirmed by sediment trap studies (Wefer 1989). Besides the high abundances in which they occur in the water column, the probability of this genus becoming incorporated in the sedimentary record is increased by its capacity to form spores.

Diatoms are rare in core MD95-2039. Slightly increased abundances do, however, occur during stages 3, 2 and 1 (Fig. 4), but the major peaks in the whole core record are at the oxygen isotope stage 6/5 and 9/10 boundaries (Terminations II and IV; Fig. 6). At these transitions diatom assemblages are dominated (>80%) by resting stages of the genus *Chaetoceros*, and these diatom maxima are exactly coincident with the major production events inferred from the C_{org} and Ba/Al records of this core.

Core MD95-2039 is one of a set of four IMAGES cores taken in two slope transects at 40°30′N and 37°50′N respectively. Similar peaks in diatom abundance are present at Termination II in the deeper (>3.1 km) cores on both transects (MD95-2039, MD95-2042), but not in the two shallower (<2.4 km) cores (MD95-2040, MD95-2041) from either transect (Knaack *et al.* 1998 and unpublished IGM-DGM data). This lack of diatoms in the inshore cores at Termination II is puzzling when the diatom spike found in both offshore cores is mainly composed of coastal upwelling-related forms. It may merely reflect a pulse of increased primary production and export flux that is only preserved in the offshore cores due to differences in the silica content of bottom waters in the region. Such a vertical zonation of differences in bottom water chemistry can be envisaged from the findings of Adkins *et al.* (1997), who have demonstrated that abrupt changes in deep water flow are associated with the beginnings and ends of interglacial periods on the Bermuda Rise.

The mechanism of productivity maxima at glacial/interglacial transitions?

The evidence is for pulses of productivity during the episodic 120+m rises in sea level at the ends of glacial periods. The possibilities seem to be first increased upwelling-driven productivity as a consequence of reorganization in ocean circulation, which appears most likely because of the association of the predominant diatom with upwelling as discussed above. At present upwelling on both the Portuguese and NW African margins is part of the Canaries Current upwelling system, but this was not the case in glacial times (Seidov & Haupt 1997). The pulses may be associated in some way with re-establishment of the Canaries Current system at Terminations, as has been observed elsewhere in the deep Atlantic (Adkins *et al.* 1997). The second alternative is increased nutrient input at times of deglaciation, either through direct run-off from land or as a result of flooding of shelves by a rising sea level. Fresh water returned to the ocean at the ends of glacial periods originates not only from melting high-latitude ice, but also from melting of terrestrial ice and permafrost. Such meltwaters making their way over land to the sea, and the resultant flooding of low-lying coastal areas which have been exposed for tens of thousands of years during glacial times, may develop high nutrient levels in coastal zone waters. This latter explanation might be expected to be local and coastal, and therefore is not an attractive explanation for the observations of Kasten *et al.* (1997) in more open ocean settings.

Conclusions

A single long core on the Iberian margin has been investigated by isotopic, geochemical, micropalaeontological and mineralogical methods. The presence of Heinrich Event layers, radiocarbon dating and the benthic foraminifera $\delta^{18}O$ record allow the development of a satisfactory depth/age model for the core, despite its rapid and time variable accumulation rate. The $CaCO_3$ content record of the core exhibits frequencies of the earth's orbital precession, obliquity and eccentricity, but these are a consequence of clay input variations rather than productivity changes. The most dramatic productivity changes in the core occur at glacial/interglacial transitions, and are expressed as simultaneous maxima in the C_{org}, biogenic Ba and diatom records.

References

ABRANTES, F. 1988. Diatom assemblages as upwelling indicators in surface sediments in Portugal. *Marine Geology*, **85**, 15–39.

—— 1990. Increased upwelling off Portugal during the last glaciation: Diatom evidence. *Marine Micropaleontology*, **17**, 285–310.

——, BAAS, J., HAFLIDASON, H., RASMUSSEN, T., KLITGAARD, D., LONCARIC, N. & GASPAR, L. 1998. Sediment fluxes along the northeastern European Margin: inferring hydrological changes between 20 and 8 ky. *Marine Geology*, **152**, 7–23.

ADKINS, J.F., BOYLE, E.A., KEIGWIN, L. & CORTIJO, E. 1997. Variability of the North Atlantic thermohaline circulation during the last interglacial period. *Nature*, **390**, 154–156.

BAAS, J.H., MEINERT, J., ABRANTES, F. & PRINS, A. 1997. Late Quaternary sedimentation on the Portuguese continental margin: climate-related processes and products. *Palaeogeography, Palaeoclimatology, Palaeoecology*, **130**, 1–23.

BACON, M.P. 1984. Glacial to interglacial changes in carbonate and clay sedimentation in the Atlantic Ocean estimated from ^{230}Th measurements. *Isotope Geoscience*, **2**, 97–111.

BARD, E. 1988. Correction of accelerator mass spectrometry ^{14}C ages measured in planktonic foraminifera: Paleoceanographic implications. *Paleoceanography*, **3**, 635–645.

——, ARNOLD, M., FAIRBANKS, R.G. & HAMELIN, B. 1993. ^{230}Th- ^{234}U and ^{14}C ages obtained by mass spectrometry on corals. *Radiocarbon*, **35**, 191–200.

BARDE, M.-F. 1981. Les diatomees des sediments actuels et du Quaternaire superieur de l'Atlantique Nord-Oriental. Interet Hydrologique et Climatique. *Bulletin Institute Géologique Bassin d'Aquitaine*, **29**, 85–111.

BASSINOT, F. & LABEYRIE, L. 1996. IMAGES MD 101 a bord du *Marion Dufresne* du 29 Mai au 11 Juillet 1995. *Publication de l'Institut Francais pour la Recherche et la Technologie Polaires*, No. 96–1.

——, ——, VINCENT, E., QUIDELLEUR, X., SHACKLETON, N.J. & LANCELOT, Y. 1994. The astronomical theory of climate and the age of the Brunhes-Matuyama magnetic reversal. *Earth and Planetary Science Letters*, **126**, 91–108.

BETZER, P.R., SHOWERS, W.J., LAWS, E.A., WINN, C.D., DITULLIO, G.R. & KROOPNICK, P.M. 1984. Primary productivity and particle fluxes on a transect of the equator at 153°W in the Pacific Ocean. *Deep-Sea Research*, **31**, 1–11.

BERGER, A. & LOUTRE, M.F. 1991. Insolation values for the climate of the last 10 My. *Quaternary Science Reviews*, **10**, 297–317.

BISHOP, J.K.B. 1988. The barite-opal-organic carbon association in oceanic particulate matter. *Nature*, **332**, 341–343.

BOND, G., BROECKER, W., JOHNSEN, S., MCMANUS, J., LABEYRIE, L., JOUZEL, J. & BONANI, G. 1993. Correlations between climate records from North Atlantic sediments and Greenland ice. *Nature*, **365**, 143–147.

——, HEINRICH, H., LABEYRIE, L. & 11 OTHERS 1992. Evidence for massive discharges of icebergs into the North Atlantic ocean during the last glacial period. *Nature*, **360**, 245–249.

BROECKER, W.S. & VAN DONK, J. 1970. Insolation changes, ice volumes, and the O^{18} record in deep-sea cores. *Reviews of Geophysics and Space Physics*, **8**, 169–198.

BRUMMER, G.J.A. & VAN EIJDEN, A.J.M. 1992. 'Blue ocean' palaeoproductivity estimates from pelagic carbonate mass accumulation rates. *Marine Micropaleontology*, **19**, 99–117.

BRUMSACK, H.J. 1986. The inorganic geochemistry of Cretaceous black shales (DSDP Leg 41) in comparison to modern upwelling sediments from the Gulf of California. *In*: SUMMERHAYES, C.P. & SHACKLETON, N.J. (eds) *North Atlantic Paleoceanography*. Geological Society Special Publication No. 21, pp. 447–462.

CHAN, L.H., EDMOND, J.M., STALLARD, R.F., BROECKER, W.S., CHUNG, Y.-C., WEISS, R.F. & KU, T.L. 1976. Radium and barium at GEOSECS stations in the Atlantic and Pacific. *Earth and Planetary Science Letters*, **32**, 258–267.

CLIMAP PROJECT MEMBERS. 1976. The surface of the ice-age earth. *Science*, **191**, 1131–1137.

CORTIJO, E., LABEYRIE, L., VIDAL, L., VAUTRAVERS, M., CHAPMAN, M., DUPLESSEY, J.-C., ELLIOT, M., ARNOLD, M., TURON, J.-L. & AUFFRET, G. 1997. Changes in sea surface hydrology associated with Heinrich event 4 in the North Atlantic Ocean between 40° and 60°N. *Earth and Planetary Science Letters*, **146**, 29–45.

DONAHUE, J.G. 1970. Pleistocene diatoms as climatic indicators in North Pacific sediments. *Geological Society America Memoir*, **426**, 121–138.

DYMOND, J. & COLLIER, R. 1996. Particulate barium fluxes and their relationships to biological productivity. *Deep-Sea Research II*, **43**, 1283–1308.

——, SUESS, E. & LYLE, M. 1992. Barium in deep-sea sediment: A geochemical proxy for paleoproductivity. *Paleoceanography*, **7**, 163–181.

GASPAR, L., ABRANTES, F. & LEBREIRO, S. 1996. Nature and Origin of Dolomite within the Portuguese Margin Sediments for the last 30 kyrs. ENAM I Final meeting, Geilo, Norway. pp. 22.

GIBBS, R.J. 1981. Sites of river-derived sedimentation in the ocean. *Geology*, **9**, 77–80.

GOLDBERG, E.D. & ARRHENIUS, G.O.S. 1958. Chemistry of Pacific pelagic sediments. *Geochimica et Cosmochimica Acta*, **13**, 153–212.

GROUSSET, F.E., LABEYRIE, L., SINKO, J.A., CREMER, M., BOND, G., DUPRAT, J., CORTIJO, E. & HUON, S. 1993. Patterns of ice-rafted detritus in the glacial North Atlantic (40–55°N). *Paleoceanography*, **8**, 175–192.

HARRIS, P.G., ZHAO, M., ROSELL-MELE, A., TIEDEMANN, R., SARNTHEIN, M. & MAXWELL, J.R. 1996. Chlorin accumulation rate as a proxy for Quaternary marine productivity. *Nature*, **383**, 63–65.

HEINRICH, H. 1988. Origin and consequences of cyclic ice rafting in the northeast Atlantic Ocean during the past 130,000 years. *Quaternary Research*, **29**, 142–152.

HULSEMANN, J. 1966. On the routine analysis of carbonates in unconsolidated sediments. *Journal of Sedimentary Petrology*, **36**, 622–625.

IMBRIE, J., HAYS, J.D., MARTINSON, D.G. & 6 OTHERS 1984. The orbital theory of Pleistocene climate: Support from a revised chronology of the marine δ18O record. *In* BERGER, A. L., *ET AL.* (eds) *Milankovitch and Climate, Part 1.* Reidel, The Netherlands, 269–305.

——, BOYLE, E.A., CLEMENS, S.C. & 15 OTHERS 1992. On the structure and origin of major glaciation cycles. 1. Linear responses to Milankovitch forcing. *Paleoceanography*, **7**, 701–738.

JARVIS, I. 1992. Sample preparation for ICP-MS. *In* JARVIS, K.E., GRAY, A.L. & HOUK, R.S. (eds) *Handbook of Inductively Coupled Plasma Mass Spectrometry*. Blackie, Glasgow, 172–224.

JUNG, S.J.A. 1996. Wassermassenaustausch zwischen dem NE-Atlantik und dem Europäischen Nordmeer während der letzten 300 000/80 000 Jahre im Abbild stabiler O- und C-Isotope. Repts. Spec. Res. Progr. 313, Univ. Kiel **61**, 1–104.

KANAYA, T. & KOIZUMI, I. 1966. Interpretation of diatom Thanatocoenoses from the North Pacific applied to a study of core V20-130. (Studies of a Deep-sea core V20-130. Part IV). *Science Reports Tohoku University*, **37**, 89–130.

KASTEN, S., RUHLEMANN, C., HAESE, R. & 5 OTHERS 1997. Barium spikes at glacial terminations in sediments of the equatorial Atlantic Ocean—Effect of nonsteady-state diagenesis? (Abstract OS52B-12, AGU 1997 Fall Meeting). *EOS*, **78**, 392.

KIEFER, T. 1998. Produktivität und Temperaturen im subtropischen Nordatlantik: zyklische und abrupte Veraenderungen im späten Quartär. *Reprs. Geol.-Paläontol. Inst. Univ. Kiel*, **90**, 1–127.

——, ABRANTES, F., SARNTHEIN, M., WEINELT, M. & LABEYRIE, L. 1995. Prominent Productivity Spikes in the Subtropical North Atlantic Parallel Heinrich Meltwater Events. *ICP V Program & Abstracts*: 85.

KNAACK, J.J., VAQUEIRO, S., GASPAR, L. & 8 OTHERS 1998. Productivity variations off Portugal during the last 350,000 years: Diatom and geochemical evidence. PAGES meeting Program & Abstracts.

KUDRASS, H.R. 1973. Sedimentation am Kontinentalhang vor Portugal und Marokko im Spätpleistozän und Holozän. 'Meteor' Forschungs-Ergebnisse, **C13**, 1–63.

LAJ, C., MAZAUD, A. & DUPLESSY, J.-C. 1996. Geomagnetic intensity and 14C abundance in the atmosphere and ocean during the past 50 ky. *Geophysical Research Letters*, **23**, 2045–2048.

LEBREIRO, S.M., MORENO, J.C., MCCAVE, I.N. & WEAVER, P.P.E. 1996. Evidence for Heinrich Layers off Portugal (Tore Seamount: 39°N, 12°W). *Marine Geology*, **131**, 47–56.

——, ——, ABRANTES, F. & PFLAUMANN, U. 1997. Productivity and paleoceanographic implications on the Tore Seamount (Iberian Margin) during the last 225 kyrs: foraminiferal evidence. *Paleoceanography*, **12**, 718–727.

LUTZE, G.F., SARNTHEIN, M., KOOPMANN, B. & PFLAUMANN, U. 1979. Meteor Core 12309: Late Pleistocene reference section for interpretation of the Neogene of site 397. *Initial Reports, Deep-Sea Drilling Program*, **47**, 727–739.

MANIGHETTI, B., MCCAVE, I.N., MASLIN, M. & SHACKLETON, N.J. 1995. Chronology for climatic change: Developing age models for the Biogeochemical Ocean Flux Study cores. *Paleoceanography*, **10**, 513–525.

MARTINSON, D.G., PISIAS, N.G., HAYES, D., IMBRIE, J., MOORE, T.C. & SHACKLETON, N.J. 1987. Age dating and the orbital theory of the ice ages: Development of a high-resolution 0 to 300,000 year chronostratigraphy. *Quaternary Research*, **27**, 1–29.

MATTHEWSON, A.P., SHIMMIELD, G.B., KROON, D. & FALLICK, A.E. 1995. A 300 ky high-resolution aridity record of the North African continent. *Paleoceanography*, **10**, 677–692.

MAYNARD, N.G. 1976. Relationship between diatoms in surface sediments of the Atlantic Ocean and the biological and physical oceanography of overlying waters. *Paleobiology*, **2**, 99–121.

MCMANUS, J.F., ANDERSON, R.F., BROECKER, W.S., FLEISHER, M.Q. & HIGGINS, S.M. 1998. Radiometrically determined sedimentary fluxes in the sub-polar North Atlantic during the last 140,000 years. *Earth and Planetary Science Letters*, **155**, 29–43.

NADEAU, M.-J., SCHLEICHER, M., GROOTES, P.M. & 5 OTHERS 1997. The Leibniz-Labor AMS facility at the Christian-Albrechts-University, Kiel, Germany. *Nuclear Instruments Methods and Physical Research B*, **123**, 22–30.

PISIAS, N.G., MARTINSON, D.G., MOORE, T.C., SHACKLETON, N.J., PRELL, W., HAYS, J. & BODEN, G. 1984. High resolution stratigraphic correlation of benthic oxygen isotopic records spanning the last 300,000 years. *Marine Geology*, **56**, 119–136.

ROHLING, E.J., FENTON, M., JORISSEN, F.J., BERTRAND, P., GANSSEN, G. & CAULET, J.P. 1998. Glacial sea level lowstands of the past 500,000 years. *Nature*, **394**, 162–165.

ROLLINSON, H. 1993. *Using geochemical data; evaluation, presentation, interpretation*. Longman, UK.

RUDDIMAN, W.F. 1977. North Atlantic ice-rafting: a major change at 75,000 years before the present. *Science*, **196**, 1208–1211.

—— & MCINTYRE, A. 1981. The North Atlantic during the last deglaciation. *Palaeogeography, Palaeoclimatology, Palaeoecology*, **35**, 145–214.

SANCETTA, C. 1979. Oceanography of the north Pacific during the last 18,000 yrs: Evidence from fossil diatoms. *Marine Micropaleontology*, **4**, 103–123.

SARNTHEIN, M., PFLAUMANN, U., ROSS, R., TIEDEMANN, R. & WINN, K. 1992. Transfer functions to reconstruct ocean palaeoproductivity: A comparison. *In* SUMMERHAYES, C.P., PRELL, W.L. & EMEIS, K.C. (eds) *Upwelling systems: Evolution since the Early Miocene.* Geological Society Special Publications, **64**, 411–427.

SCHRADER, H. & SORKNESS, R. 1991. Peruvian coastal upwelling; Late Quaternary productivity changes revealed by diatoms. *Marine Geology*, **97**, 233–249.

SEIDOV, D. & HAUPT, B.J. 1997. Simulated ocean circulation and sediment transport in the North Atlantic during the last glacial maximum and today. *Paleoceanography*, **12**, 281–305.

SHACKLETON, N.J. 1987. Oxygen isotopes, ice volume and sea level. *Quaternary Science Reviews*, **6**, 183–190.

STUIVER, M. & POLACH, H.A. 1977. Discussion: Reporting of 14C data. *Radiocarbon*, **19**, 355–363.

THOMSON, J., HIGGS, N.C. & CLAYTON, T. 1995a. A geochemical criterion for the recognition of Heinrich events and estimation of their deposition fluxes by the $(^{230}Th_{excess})_o$ profiling method. *Earth and Planetary Science Letters*, **135**, 41–56.

——, COOK, G.T., ANDERSON, R., MACKENZIE, A.B., HARKNESS, D.D. & MCCAVE, I.N. 1995b. Radiocarbon age off-sets in different-sized carbonate components of deep-sea sediments. *Radiocarbon*, **37,** 91–101.

——, NIXON, S., SUMMERHAYES, C.P., SCHÖNFELD, J., ZAHN, R. & GROOTES, P. 1999. Implications for sedimentation changes on the Iberian margin over the last two glacial/interglacial transitions from (^{230}Th$_{excess}$) systematics. *Earth and Planetary Science Letters*, **165,** 255–270.

TORRES, M.E., BRUMSACK, H.J., BOHRMANN, G. & EMEIS, K.C. 1996. Barite fronts in continental margin sediments: A new look at barium remobilisation in the zone of sulfate reduction and formation of heavy barites in diagenetic fronts. *Chemical Geology*, **127,** 125–139.

TRAUTH, M.H. & SARNTHEIN, M. 1997. Bioturbational mixing depth and carbon flux at the sea floor. *Paleoceanography*, **12,** 517–526.

VAN KREVELD, S.A., KNAPPERTSBUSCH, M., OTTENS, J., GANSSEN, G.M. & VAN HINTE, J.E. 1996. Biogenic carbonate and ice-rafted debris (Heinrich layer) accumulation in deep-sea sediments from a Northeast Atlantic piston core. *Marine Geology*, **131,** 21–46.

VIDAL, L., LABEYRIE, L., CORTIJO, E., ARNOLD, M., DUPLESSEY, J.C., MICHEL, E., BECQUE, S. & VAN WEERING, T.C.E. 1997. Evidence for changes in the North Atlantic Deep Water linked to meltwater surges during Heinrich events. *Earth and Planetary Science Letters*, **146,** 13–27.

WEFER, G. 1989. Particle flux in the ocean: Effects of episodic production. *In*: BERGER, W.H., SMETACEK, V.S. & WEFER, G. (eds) *Productivity in the Ocean: Present and Past*. Wiley, New York, 139–153.

WINN, K., SARNTHEIN, M. & ERLENKEUSER, H. 1991. δ^{18}O stratigraphy and chronology of Kiel sediment cores from the East Atlantic. *Reports Geologische-Paläontologische Institut, Universitat Kiel*, **45,** 1–99.

ZAHN, R., SCHÖNFELD, J., KUDRASS, H.-R., PARK, M.-H. & ERLENKEUSER, H. 1997. Thermohaline instability in the North Atlantic during Heinrich Events: Stable isotope and IRD records from core SO75-26KL, Portuguese Margin. *Paleoceanography*, **12,** 696–710.